
A Spike in Performance: Training Hybrid-Spiking Neural Networks with Quantized Activation Functions

Aaron R. Voelker¹ Daniel Rasmussen¹ Chris Eliasmith^{1,2}

Abstract

The machine learning community has become increasingly interested in the energy efficiency of neural networks. The Spiking Neural Network (SNN) is a promising approach to energy-efficient computing, since its activation levels are quantized into temporally sparse, one-bit values (i.e., “spike” events), which additionally converts the sum over weight-activity products into a simple addition of weights (one weight for each spike). However, the goal of maintaining state-of-the-art (SotA) accuracy when converting a non-spiking network into an SNN has remained an elusive challenge, primarily due to spikes having only a single bit of precision. Adopting tools from signal processing, we cast neural activation functions as quantizers with temporally-diffused error, and then train networks while smoothly interpolating between the non-spiking and spiking regimes. We apply this technique to the Legendre Memory Unit (LMU) to obtain the first known example of a hybrid SNN outperforming SotA recurrent architectures—including the LSTM, GRU, and NRU—in accuracy, while reducing activities to at most 3.74 bits on average with 1.26 significant bits multiplying each weight. We discuss how these methods can significantly improve the energy efficiency of neural networks.

1. Introduction

The growing amount of energy consumed by Artificial Neural Networks (ANNs) has been identified as an important problem in the context of mobile, IoT, and edge applications (Moloney, 2016; Zhang et al., 2017; McKinstry et al., 2018; Wang et al., 2019; Situnayake & Warden, 2019). The vast majority of an ANN’s time and energy is consumed by the multiply-accumulate (MAC) operations implementing

the weighting of activities between layers (Sze et al., 2017). Thus, many ANN accelerators focus almost entirely on optimizing MACs (e.g. Ginsburg et al., 2017; Jouppi et al., 2017), while practitioners prune (Zhu & Gupta, 2017; Liu et al., 2018) and quantize (Gupta et al., 2015; Courbariaux et al., 2015; McKinstry et al., 2018; Nayak et al., 2019) weights to reduce the use and size of MAC arrays.

While these strategies focus on the weight matrix, the Spiking Neural Network (SNN) community has taken a different but complementary approach that instead focuses on temporal processing. The operations of an SNN are *temporally sparsified*, such that an accumulate only occurs whenever a “spike” arrives at its destination. These sparse, one-bit activities (i.e., “spikes”) not only reduce the volume of data communicated between nodes in the network (Furber et al., 2014), but also replace the multipliers in the MAC arrays with adders – together providing orders of magnitude gains in energy efficiency (Davies et al., 2018; Blouw et al., 2019).

The conventional method of training an SNN is to first train an ANN, replace the activation functions with spiking neurons that have identical firing rates (Hunsberger & Eliasmith, 2015), and then optionally retrain with spikes on the forward pass and a differentiable proxy on the backward pass (Huh & Sejnowski, 2018; Bellec et al., 2018; Zhang & Li, 2019). However, converting an ANN into an SNN often degrades model accuracy – especially for recurrent networks. Thus, multiple hardware groups have started building hybrid architectures that support ANNs, SNNs, and mixtures thereof (Liu et al., 2018; Pei et al., 2019; Moreira et al., 2020) – for instance by supporting event-based activities, fixed-point representations, and a variety of multi-bit coding schemes. These hybrid platforms present the alluring possibility to trade accuracy for energy in task-dependent ways (Anonymous, 2020). However, principled methods of leveraging such trade-offs are lacking.

In this work, we propose to our knowledge the first method of training hybrid-spiking networks (hSNNs) by smoothly interpolating between ANN (i.e., 32-bit activities) and SNN (i.e., 1-bit activities) regimes. The key idea is to interpret spiking neurons as one-bit quantizers that diffuse their quantization error across future time-steps – similar to Floyd & Steinberg (1976) dithering. This idea can be readily applied

*Equal contribution ¹Applied Brain Research Inc. ²University of Waterloo, Waterloo, ON, Canada. Correspondence to: Aaron R. Voelker <aaron.voelker@appliedbrainresearch.com>.

to any activation function at little additional cost, generalizes to quantizers with arbitrary bit-widths (even fractional), provides strong bounds on the quantization errors, and relaxes in the limit to the ideal ANN.

Our methods enable the training procedure to balance the accuracy of ANNs with the energy efficiency of SNNs by evaluating the continuum of networks in between these two extremes. Furthermore, we show that this method can train hSNNs with superior accuracy to ANNs and SNNs trained via conventional methods. In a sense, we show that it is useful to think of spiking and non-spiking networks as extremes in a continuum. As a result, the family of hSNNs captures networks with any mixture of activity quantization throughout the architecture.

2. Related Work

Related work has investigated the quantization of activation functions in the context of energy-efficient hardware (e.g., Jacob et al., 2018; McKinstry et al., 2018). Likewise, Hopkins et al. (2019) consider stochastic rounding and dithering as a means of improving the accuracy of spiking neuron models on low-precision hardware relative to their ideal ordinary differential equations (ODEs). These approaches do not account for the quantization errors that accumulate over time, whereas our proposed method keeps them bounded.

Some have viewed spiking neurons as one-bit quantizers, or analog-to-digital (ADC) converters, including Chklovskii & Soudry (2012); Yoon (2016); Ando et al. (2018); Neckar et al. (2018); Yousefzadeh et al. (2019a;b). But these methods are not generalized to multi-bit or hybrid networks, nor leveraged to interpolate between non-spiking and spiking networks during training.

There also exist other methods that introduce temporal sparsity into ANNs. One such example is channel gating (Hua et al., 2019), whereby the channels in a CNN are dynamically pruned over time. Another example is dropout (Srivastava et al., 2014) – a form of regularization that randomly drops out activities during training. The gating mechanisms in both cases are analogous to spiking neurons.

Neurons that can output multi-bit spikes have been considered in the context of packets that bundle together neighbouring spikes (Krithivasan et al., 2019). In contrast, this work directly computes the number of spikes in $\mathcal{O}(1)$ time and memory per neuron, and varies the temporal resolution during training to interpolate between non-spiking and spiking and allow optimization across the full set of hSNNs.

Our methods are motivated by some of the recent successes in training SNNs to compete with ANNs on standard machine learning benchmarks (Bellec et al., 2018; Stöckl & Maass, 2019; Pei et al., 2019). To our knowledge, this

work is the first to parameterize the activation function in a manner that places ANNs and SNNs on opposite ends of the same spectrum. We show that this idea can be used to convert ANNs to SNNs, and to train hSNNs with improved accuracy relative to pure (i.e., 1-bit) SNNs and energy efficiency relative to pure (i.e., 32-bit) ANNs.

3. Methods

3.1. Quantized Activation Functions

We now formalize our method of quantizing any activation function. In short, the algorithm quantizes the activity level and then pushes the quantization error onto the next time-step – analogous to the concept of using error diffusion to dither a one-dimensional time-series (Floyd & Steinberg, 1976). The outcome is a neuron model that interpolates an arbitrary activation function, f , between non-spiking and spiking regimes through choice of the parameter $\omega > 0$, which acts like a time-step.

3.1.1. TEMPORALLY-DIFFUSED QUANTIZER

Let x_t be the input to the activation function at a discrete time-step, $t > 0$, such that the ideal output (i.e., with unlimited precision) is $a_t = f(x_t)$. The algorithm maintains one scalar state-variable across time, v_t , that tracks the total amount of quantization error that the neuron has accumulated over time. We recommend initializing $v_0 \sim \mathcal{U}[0, 1)$ independently for each neuron. The output of the neuron, \tilde{a}_t , is determined by Algorithm 1.¹

The ideal activation, f , may be any conventional nonlinearity (e.g., tanh, sigmoid, etc.), or the time-averaged response curve corresponding to a biological neuron model (e.g., leaky integrate-and-fire) including those with multiple internal state-variables (Koch, 2004). Adaptation may also be modelled by including a recurrent connection from \tilde{a}_t to x_{t+1} (Voelker, 2019, section 5.2.1).

To help understand the relationship between this algorithm and spiking neuron models, it is useful to interpret \tilde{a}_t as the number of spikes (k) that occur across a window of time normalized by the length of this window (ω). Then $f(x_t) \times \omega$ represents the expected number of spikes across the window, and v_t tracks progress towards the next spike.

We note that Algorithm 1 is equivalent to Ando et al. (2018, Algorithm 1) where $f(x) = \max(x, 0)$ is the rectified linear (ReLU) activation function, and $\omega = 1$. Yousefzadeh et al. (2019a, Algorithm 1) extend this to represent changes in activation levels, and allow negative spikes. Still considering the ReLU activation, Algorithm 1 is again equivalent to the spiking integrate-and-fire (IF) neuron model, without

¹This algorithm, and related methods, are patent pending technologies (Voelker, 2020) of Applied Brain Research Inc.

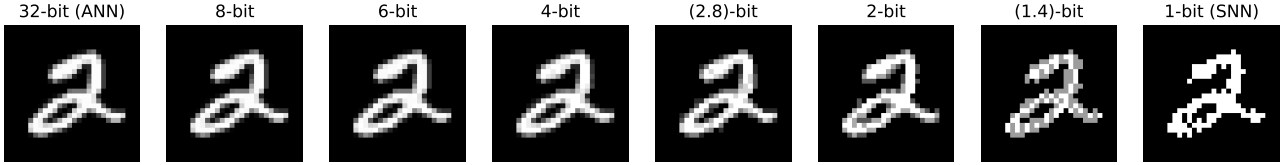


Figure 1: Visualizing the output (\tilde{a}_t) of Algorithm 1 given an MNIST digit as input (x_t). The bit-width is varied as $\omega = 2^m - 1$; $m = 32$ correspond to the activities of a 32-bit ANN, whereas $0 < m \leq 1$ correspond to those of an SNN.

Algorithm 1 Temporally-Diffused Quantizer ($f; \omega$)

Input: x_t

State: v_t

Output: \tilde{a}_t

$s \leftarrow v_{t-1} + f(x_t) \times \omega$

$k \leftarrow \lfloor s \rfloor$

$v_t \leftarrow s - k$

$\tilde{a}_t \leftarrow k/\omega$

a refractory period, a membrane voltage of v_t normalized to $[0, 1)$, a firing rate of 1 Hz, and the ODE discretized to a time-step of ω s using zero-order hold (ZOH). The ω parameter essentially generalizes the spiking model to allow multiple spikes per time-step, and the IF restriction is lifted to allow arbitrary activation functions (including leaky neurons, and those with negative spikes such as tanh).

3.1.2. SCALING PROPERTIES

We now state several important properties of this quantization algorithm (see supplementary for proofs). For convenience, we assume the range of f is scaled such that $|f(\cdot)| \leq 1$ over the domain of valid inputs (this can also be achieved via clipping or saturation).

Zero-Mean Error Supposing $v_{t-1} \sim \mathcal{U}[0, 1)$, the expected quantization error is $\mathbb{E}[\tilde{a}_t - a_t] = 0$.

Bounded Error The total quantization error is bounded by $|\sum_{t \in T} \tilde{a}_t - a_t| < \omega^{-1}$ across *any* consecutive slice of time-steps, T . As a corollary, the signal-to-noise ratio (SNR) of \tilde{a}_t scales as $\Omega(\omega)$, and this SNR may be further scaled by the time-constant of a lowpass filter (see section 3.3).

Bit-Width The number of bits required to represent \tilde{a}_t in binary is at most $\lceil \log_2(\omega + 1) \rceil$ if f is non-negative (plus a sign bit if f can be negative).

ANN Regime As $\omega \rightarrow \infty$, $\tilde{a}_t \rightarrow a_t$, hence the activation function becomes equivalent to the ideal $f(\cdot)$.

SNN Regime When $\omega \leq 1$, the activation function becomes a conventional spiking neuron since it outputs either zero or a spike (ω^{-1}) if f is non-negative (and optionally a negative spike if f is allowed to be negative).

Temporal Sparsity The spike count scales as $\mathcal{O}(\omega)$.

To summarize, the choice of ω results in activities that require $\mathcal{O}(\log \omega)$ bits to represent, while achieving an SNR of $\Omega(\omega)$ relative to the ideal function. The effect of the algorithm is depicted in Figure 1 for various ω .

3.1.3. BACKPROPAGATION TRAINING

To train the network via backpropagation, we make the simplifying assumption that $(v_{t-1}, v_t) \sim \mathcal{U}[0, 1)$ are independent random variables, which implies that $\tilde{a}_t = a_t + \eta$ where $\eta \sim \mathcal{T}(-\omega^{-1}, \omega^{-1})$ is zero-mean noise with a symmetric triangular distribution (see supplementary). This justifies assigning a gradient of zero to η . The forward pass uses the quantized activation function to compute the true error for the current ω , while the backward pass uses the gradient of f (independently of ω). In summary, our scheme accounts for the temporal mechanisms of spike generation, but allows the gradient to skip over the sequence of operations that keep the total spike noise bounded by ω^{-1} .

3.2. Legendre Memory Unit

As an example application of these methods we will use the Legendre Memory Unit (LMU; Voelker et al., 2019) – a new type of Recurrent Neural Network (RNN) that efficiently orthogonalizes the continuous-time history of some signal, $u(t) \in \mathbb{R}$, across a sliding window of length $\theta > 0$. The network is characterized by the following d coupled ODEs:

$$\theta \dot{\mathbf{m}}(t) = \mathbf{A}\mathbf{m}(t) + \mathbf{B}u(t) \quad (1)$$

where $\mathbf{m}(t) \in \mathbb{R}^d$ is a d -dimensional memory vector, and (\mathbf{A}, \mathbf{B}) have a closed-form solution (Voelker, 2019):

$$\mathbf{A} = [a]_{ij} \in \mathbb{R}^{d \times d}, \quad a_{ij} = (2i + 1) \begin{cases} -1 & i < j \\ (-1)^{i-j+1} & i \geq j \end{cases}$$

$$\mathbf{B} = [b]_i \in \mathbb{R}^{d \times 1}, \quad b_i = (2i + 1)(-1)^i. \quad (2)$$

The key property of this dynamical system is that \mathbf{m} represents sliding windows of u via the [Legendre \(1782\)](#) polynomials up to degree $d - 1$:

$$u(t - \theta') \approx \sum_{i=0}^{d-1} \mathcal{P}_i \left(\frac{\theta'}{\theta} \right) m_i(t), \quad 0 \leq \theta' \leq \theta \quad (3)$$

$$\mathcal{P}_i(r) = (-1)^i \sum_{j=0}^i \binom{i}{j} \binom{i+j}{j} (-r)^j$$

where $\mathcal{P}_i(r)$ is the i^{th} shifted Legendre polynomial ([Rodrigues, 1816](#)). Thus, nonlinear functions of \mathbf{m} correspond to functions across windows of length θ projected onto the Legendre basis.

Discretization We map these equations onto the state of an RNN, $\mathbf{m}_t \in \mathbb{R}^d$, given some input $u_t \in \mathbb{R}$, indexed at discrete moments in time, $t \in \mathbb{N}$:

$$\mathbf{m}_t = f_m(\bar{\mathbf{A}}\mathbf{m}_{t-1} + \bar{\mathbf{B}}u_t) \quad (4)$$

where $(\bar{\mathbf{A}}, \bar{\mathbf{B}})$ are the ZOH-discretized matrices from equation 2 for a time-step of $\bar{\theta}^{-1}$, such that $\bar{\theta}$ is the desired memory length expressed in discrete time-steps. In the ideal case, $f_m(\cdot)$ should be the identity function. For our hSNNs, we clip and then quantize $f_m(\cdot)$ using Algorithm 1.

Architecture The LMU takes an input vector, \mathbf{x}_t , and generates a hidden state. The hidden state, $\mathbf{h}_t \in \mathbb{R}^n$, and memory vector, $\mathbf{m}_t \in \mathbb{R}^d$, correspond to the activities of two neural populations that we will refer to as the hidden neurons and memory neurons, respectively. The hidden neurons mutually interact with the memory neurons in order to compute nonlinear functions across time, while dynamically writing to memory. The state is a function of the input, previous state, and current memory:

$$\mathbf{h}_t = f_h(\mathbf{W}_x\mathbf{x}_t + \mathbf{W}_h\mathbf{h}_{t-1} + \mathbf{W}_m\mathbf{m}_t) \quad (5)$$

where $f_h(\cdot)$ is some chosen nonlinearity—to be quantized using Algorithm 1—and $\mathbf{W}_x, \mathbf{W}_h, \mathbf{W}_m$ are learned weights. The input to the memory is:

$$u_t = \mathbf{e}_x^\top \mathbf{x}_t + \mathbf{e}_h^\top \mathbf{h}_{t-1} + \mathbf{e}_m^\top \mathbf{m}_{t-1} \quad (6)$$

where $\mathbf{e}_x, \mathbf{e}_h, \mathbf{e}_m$ are learned vectors.

3.3. Synaptic Filtering

SNNs commonly apply a synapse model to the weighted summation of spike-trains. This filters the input to each neuron over time to reduce the amount of spike noise ([Dayan & Abbott, 2001](#)). The synapse is most commonly modelled as a lowpass filter, with some chosen time-constant τ , whose effect is equivalent to replacing each spike with an exponentially decaying kernel, $h(t) = \tau^{-1}e^{-t/\tau}$ ($t \geq 0$).

By lowpass filtering the activities, the SNR of Algorithm 1 is effectively boosted by a factor of $\Omega(\tau)$ relative to the filtered ideal, since the filtered error becomes a weighted time-average of the quantization errors (see supplementary). Thus, we lowpass filter the inputs into both $f_m(\cdot)$ and $f_h(\cdot)$.

To account for the temporal dynamics introduced by the application of a lowpass filter, [Voelker & Eliasmith \(2018, equation 4.7\)](#) prove that the LMU’s discretized state-space matrices, $(\bar{\mathbf{A}}, \bar{\mathbf{B}})$, should be exchanged with $(\bar{\mathbf{A}}^H, \bar{\mathbf{B}}^H)$:

$$\bar{\mathbf{A}}^H = \frac{1}{1 - e^{-1/\bar{\tau}}} (\bar{\mathbf{A}} - e^{-1/\bar{\tau}}I) \quad (7)$$

$$\bar{\mathbf{B}}^H = \frac{1}{1 - e^{-1/\bar{\tau}}} \bar{\mathbf{B}}$$

where $\bar{\tau}$ is the time-constant (in discrete time-steps) of the ZOH-discretized lowpass that is filtering the input to f_m .

To summarize, the architecture that we train includes a nonlinear layer (\mathbf{h}) and a linear layer (\mathbf{m}), each of which has synaptic filters. The recurrent and input weights to \mathbf{m} are fixed to $\bar{\mathbf{A}}^H$ and $\bar{\mathbf{B}}^H$, and are not trained. All other connections are trained.

3.4. SNR Scheduling

To interpolate between ANN and SNN regimes, we set ω differently from one training epoch to the next, in an analogous manner to scheduling learning rates. Since ω is exponential in bit-precision, we vary ω on a logarithmic scale across the interval $[\omega_h, \omega_l]$, where ω_h is set to achieve rapid convergence during the initial stages of training, and ω_l depends on the hardware and application. Once $\omega = \omega_l$, training is continued until validation error stops improving, and only the model with the lowest validation loss during this fine-tuning phase is saved.

We found that this method of scheduling ω typically results in faster convergence rates versus the alternative of starting ω at its final value. We also observe that the SNR of $f_m(\cdot)$ is far more critical than the SNR of $f_h(\cdot)$, and thus schedule the two differently (explained below).

4. Experiments

To facilitate comparison between the “Long Short-Term Memory Spiking Neural Network” (LSNN) from [Bellec et al. \(2018\)](#), and both spiking and non-spiking LMUs ([Voelker et al., 2019](#)), we consider the sequential MNIST (sMNIST) task and its permuted variant (psMNIST; [Le et al., 2015](#)). For sMNIST, the pixels are supplied sequentially in a time-series of length 28^2 . Thus, the network must maintain a memory of the relevant features while simultaneously computing across them in time. For psMNIST, all of the sequences are also permuted by an unknown fixed permutation matrix, which distorts the temporal structure

Table 1: Performance of RNNs on the sequential MNIST task.

NETWORK	TRAINABLE	WEIGHTS	NONLINEARITIES	STATE	LEVELS	STEPS	TEST (%)
LSTM	67850	67850	384 SIGMOID, 128 TANH	256	2^{32}	784	98.5
LMU	34571	51083	128 SIGMOID	256	2^{32}	784	98.26
hSLMU	34571	51083	128 LIF, 128 IF	522	2-5	784	97.26
LSNN	68210	8185	120 LIF, 100 ADAPTIVE	≥ 550	2	1680	96.4

in the sequences and significantly increases the difficulty of the task. In either case, the network outputs a classification at the end of each input sequence. For the output classification, we take the argmax over a dense layer with 10 units, with incoming weights initialized using the Xavier uniform distribution (Glorot & Bengio, 2010). The network is trained using the categorical crossentropy loss function (fused with softmax).

All of our LMU networks are built in Nengo (Bekolay et al., 2014) and trained using Nengo-DL (Rasmussen, 2019). The 50k “lost MNIST digits” (Yadav & Bottou, 2019)² are used as validation data to select the best model. All sequences are normalized to $[-1, 1]$ via fixed linear transformation $(2x/255 - 1)$. We use a minibatch size of 500, and the Adam optimizer (Kingma & Ba, 2014) with all of the default hyperparameters ($\alpha = 0.001$, $\beta_1 = 0.9$, $\beta_2 = 0.999$).

To quantize the hidden activations, we use the leaky integrate-and-fire (LIF) neuron model with a refractory period of 1 time-step and a leak of 10 time-steps (corresponding to Nengo’s defaults given a time-step of 2 ms), such that its response curve is normalized to $0 \leq f_h(\cdot) < 1$. The input to each LIF neuron is biased such that $f(x) = 0 \iff x \leq 0$, and scaled such that $f(1) = e/(1 + e)$ (see supplementary). During training, the ω for $f_h(\cdot)$ is interpolated across $[16, 1]$. Thus, the hidden neurons in the fully trained networks are conventional (1-bit) spiking neurons.

To quantize the memory activations, we use $f_m(x) = x.\text{clip}(-1, +1)$, which is analogous to using IF neurons that can generate both positive and negative spikes. To maintain accuracy, the ω for $f_m(\cdot)$ is interpolated across $[32, 2]$ for sMNIST, and across $[4080, 255]$ for psMNIST. We provide details regarding the effect of these choices on the number of possible activity levels for the memory neurons, and discuss the impact this has on MAC operations as well as the consequences for energy-efficient neural networks.

The synaptic lowpass filters have a time-constant of 200 time-steps for the activities projecting into $f_m(\cdot)$, and 10 time-steps for the activities projecting into $f_h(\cdot)$. The output layer also uses a 10 time-step lowpass filter. We did not experiment with any other choice of time-constants.

²This set does not overlap with MNIST’s train or test sets.

All weights are initialized to zero, except: e_x is initialized to 1, \mathbf{W}_m is initialized using the Xavier normal distribution (Glorot & Bengio, 2010), and $(\bar{\mathbf{A}}^H, \bar{\mathbf{B}}^H)$ are initialized according to equation 7 and left untrained. L2-regularization ($\lambda = 0.01$) is added to the output vector. We did not experiment with batch normalization, layer normalization, dropout, or any other regularization techniques.

4.1. Sequential MNIST

4.1.1. STATE-OF-THE-ART

The LSTM and LSNN results shown in Table 1 have been extended from Bellec et al. (2018, Tables S1 and S2). We note that these two results (98.5% and 96.4%) represent the best test accuracy among 12 separately trained models, without any validation. The mean test performance across the same 12 runs are 79.8% and 93.8% for the LSTM and LSNN, respectively.

The LSTM consists of only 128 “units,” but is computationally and energetically intensive since it maintains a 256-dimensional vector of 32-bit activities that are multiplied with over 67k weights. The LSNN improves this in two important ways. First, the activities of its 220 neurons are all one bit (i.e., spikes). Second, the number of parameters are pruned down to just over 8k weights. Thus, each time-step consists of at most 8k synaptic operations that simply add a weight to the synaptic state of each neuron, followed by local updates to each synapse and neuron model.

However, the LSNN suffers from half the throughput (each input pixel is presented for two time-steps rather than one), a latency of 112 additional time-steps to accumulate the classification after the image has been presented (resulting in a total of $2 \times 28^2 + 112 = 1680$ steps), and an absolute 2.1% decrease in test accuracy. In addition, at least 550 state-variables (220 membrane voltages, 100 adaptive thresholds, 220 lowpass filter states, 10 output filters states, plus state for an optional delay buffer attached to each synapse) are required to maintain memory between time-steps. The authors state that the input to the LSNN is preprocessed using 80 more neurons that fire whenever the pixel crosses over a fixed value associated with each neuron, to obtain “some-what better performance.”

Table 2: Performance of RNNs on the permuted sequential MNIST task.

NETWORK	TRAINABLE	WEIGHTS	NONLINEARITIES	BIT-WIDTH	SIGNIFICANT BITS	TEST (%)
LSTM	163610	163610	600 SIGMOID, 200 TANH	32	N/A	89.86
LMU	102027	167819	212 TANH	32	N/A	97.15
hSLMU	102239	168031	212 LIF, 256 IF	3.74	1.26	96.83

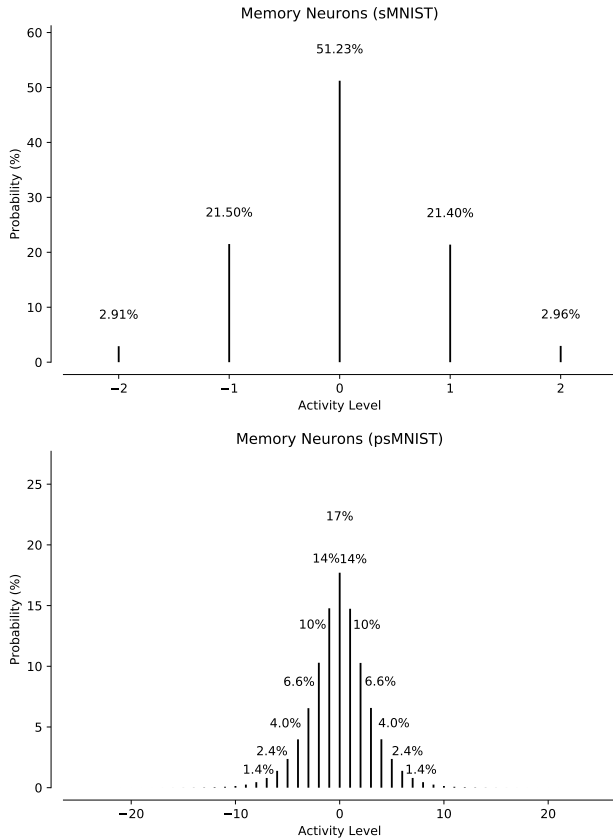


Figure 2: Distribution of activity levels for the memory neurons, $f_m(\cdot)$, in the hsLMU network solving the sMNIST task (Top; see Table 1) and the psMNIST task (Bottom; see Table 2).

4.1.2. NON-SPIKING LMU

The non-spiking LMU is the Nengo implementation from Voelker et al. (2019)³ with $n = 128$ and $d = 128$, the sigmoid activation chosen for $f_h(\cdot)$, and a trainable bias vector added to the hidden neurons.

This network obtains a test accuracy of 98.26%, while using only 128 nonlinearities, and training nearly half as many weights as the LSTM or LSNN. However, the MAC operations are still a bottleneck, since each time-step requires multiplying a 256-dimensional vector of 32-bit activities

³<https://www.nengo.ai/nengo-dl/examples/lmu.html>

with approximately 51k weights (including $\bar{\mathbf{A}}^H$ and $\bar{\mathbf{B}}^H$).

4.1.3. HYBRID-SPIKING LMU

To simplify the MAC operations, we quantize the activity functions and filter their inputs (see section 3). We refer to this as a “hybrid-spiking LMU” (hsLMU) since the hidden neurons are conventional (i.e., one-bit) spiking LIF neurons, but the memory neurons can assume a multitude of distinct activation levels by generating multiple spikes per time-step.

By training until $\omega = 2$ for $f_m(\cdot)$, each memory neuron can spike at 5 different activity levels (see Figure 2; Top). We remark that the distribution is symmetric about zero, and “prefers” the zero state (51.23%), since equation 1 has exactly one stable point: $\mathbf{m}(t) = \mathbf{0}$. As well, the hidden neurons spike only 36.05% of the time. As a result, the majority of weights are not needed on any given time-step. Furthermore, when a weight is accessed, it is simply added for the hidden activities, or multiplied by an element of $\{-2, -1, +1, +2\}$ for the memory activities.

These performance benefits come at the cost of a 1% decrease in test accuracy, and additional state and computation—local to each neuron—to implement the low-pass filters and Algorithm 1. Specifically, this hsLMU requires 522 state-variables (256 membrane voltages, 256 lowpass filters, and 10 output filters). This network outperforms the LSNN, does not sacrifice throughput nor latency, and does not require special preprocessing of the input data.

4.2. Permuted Sequential MNIST

4.2.1. STATE-OF-THE-ART

Several RNN models have been used to solve the psMNIST task (Chandar et al., 2019), with the highest accuracy of 97.15% being achieved by an LMU (Voelker et al., 2019) of size $n = 212$, $d = 256$. The LMU result, and the LSTM result from Chandar et al. (2019), are reproduced in Table 2.

4.2.2. HYBRID-SPIKING LMU

We consider the same network from section 4.1.3, scaled up to $n = 212$ and $d = 256$. Consistent with the previous hsLMU, the hidden neurons are spiking LIF, and the memory neurons are multi-bit IF neurons that can generate multiple positive or negative spikes per step. In particular,

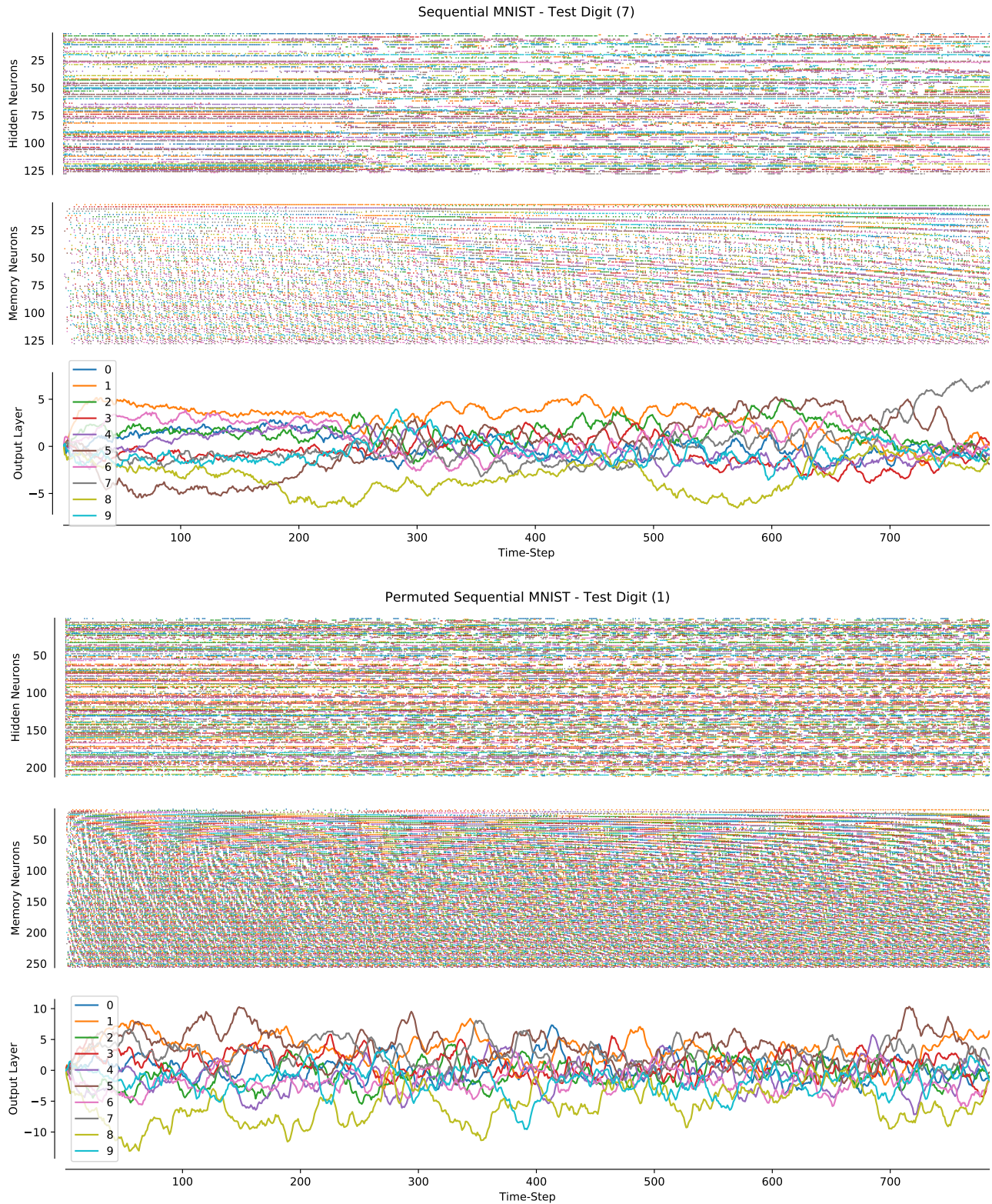


Figure 3: An example of each hybrid-spiking Legendre Memory Unit (hsLMU) network producing the correct classification given a test digit for the sMNIST task (Top; see Table 1) and the psMNIST task (Bottom; see Table 2). The recurrent network consists of one-bit spiking LIF neurons (representing h_t) coupled with multi-bit spiking IF neurons (representing m_t). Classifications are obtained by taking an argmax of the output layer on the final time-step of each sequence.

by training until $\omega = 255$ for $f_m(\cdot)$, each memory neuron can spike between -24 and $+26$ times (inclusive) per step for a total of 50 distinct activity levels, which requires 6 bits to represent.

Again, the distribution of memory activities are symmetric about zero, and 17.71% of the time the neurons are silent. The 1-bit hidden neurons spike 40.24% of the time. We note that the hsLMU uses 212 more parameters than the LMU from Voelker et al. (2019), as the latter does not include a bias on the hidden nonlinearities.

To quantify the performance benefits of low-precision activities, we propose the following two metrics. The first is the worst-case number of bits required to communicate the activity of each neuron, in this case 1 for the hidden neurons and 6 for the memory neurons, which has a weighted average of approximately 3.74 bits. The second is the number of bits that are significant (i.e., after removing all of the trailing zero bits, and including a sign bit for negative activities), which has a weighted average of approximately 1.26 bits.

The “bit-width” metric is useful for determining the worst-case volume of spike traffic on hardware where the size of the activity vectors are user-configurable (Furber et al., 2014; Liu et al., 2018), and for hardware where the quantization of activities leads to quadratic improvements in silicon area and energy requirements (McKinstry et al., 2018). The “significant bits” metric reflects how many significant bits are multiplied with each weight, which is important for hardware where bit-flips in the datapath correlate with energy costs (Li et al., 2019), or hardware that is optimized for integer operands close to zero. For instance, a value of 1 for this metric would imply that each MAC, on average, only needs to accumulate its weight (i.e., no multiply is required). These performance benefits come at the cost of a 0.32% decrease in test accuracy, which still outperforms all other RNNs considered by Chandar et al. (2019); Voelker et al. (2019) apart from the LMU, while using comparable resources and parameter counts.

Interestingly, for the sMNIST network in section 4.1.3, the bit-width metric is exactly 2 (as there are an equal number of hidden (1-bit) and memory (3-bit) neurons). The significant bits for that network is 0.58, because a majority of the neurons are inactive on each time step.

5. Discussion

Although the biological plausibility of a neuron that can output more than one spike “at once” is questionable, it is in fact mathematically equivalent to simulating the neuron with a time-step of ω and bundling the spikes together (Krithivasan et al., 2019). Consequently, all of the networks we consider here can be implemented in 1-bit spiking networks, although with an added time cost. This is similar to the LSNN’s ap-

proach of simulating the network for two time-steps per image pixel, but does not incur the same cost in throughput. Alternatively, a space cost can be paid by replicating the neuron ω times and uniformly spacing the initial v_0 (not shown). Likewise, negative spikes are a more compact and efficient alternative to duplicating the neurons and mirroring their activation functions.

Our methods are convenient to apply to the LMU because equation 7 accounts for the dynamics of the lowpass filter, and the \mathbf{m}_t vector naturally prefers the zero (i.e., silent) state. At the same time, it is a challenging test for the theory, since we do not train the LMU matrices, which are primarily responsible for accuracy on psMNIST (Voelker et al., 2019), and RNNs tend to accumulate and propagate their errors over time. Notably, the method of Algorithm 1 can be applied to other neural network architectures, including feed-forward networks.

6. Conclusions

We have presented a new algorithm and accompanying methods that allow interpolation between spiking and non-spiking networks. This allows the training of hSNNs, which can have mixtures of activity quantization, leading to computationally efficient neural network implementations. We have also shown how to incorporate standard SNN assumptions, such as the presence of a synaptic filter.

We demonstrated the technique on the recently proposed LMU, and achieved better than state-of-the-art results on sMNIST than a spiking network. Additionally, on the more challenging psMNIST task the reported accuracy of the spiking network is better than any non-spiking RNN apart from the original LMU (Chandar et al., 2019; Voelker et al., 2019).

However, our focus here is not on accuracy per se, but efficient computation. In this context, the training procedure enables us to leverage the accuracy of ANNs and the energy efficiency of SNNs by scheduling training to evaluate a series of networks in between these two extremes. In the cases we considered, we reduced the activity to 2–6 bits on average, saving at least 26 bits over the standard LMU implementation with minimal impact on accuracy. While difficult to convert these metrics to energy savings in a hardware-agnostic manner, such optimizations can benefit both spiking and non-spiking architectures.

We anticipate that techniques like those we have outlined here will become more widely used as the demands of edge computing continue to grow. In such power-constrained contexts, extracting as much efficiency as possible, while retaining sufficient accuracy, is central to the efforts involved in co-designing both algorithms and hardware for neural network workloads.

References

- Ando, K., Ueyoshi, K., Oba, Y., Hirose, K., Uematsu, R., Kudo, T., Ikebe, M., Asai, T., Takamaeda-Yamazaki, S., and Motomura, M. Dither NN: An accurate neural network with dithering for low bit-precision hardware. In *2018 International Conference on Field-Programmable Technology (FPT)*, pp. 6–13. IEEE, 2018.
- Anonymous. Event-driven signal processing with neuromorphic computing systems. In *45th International Conference on Acoustics, Speech, and Signal Processing*. IEEE, 2020.
- Bekolay, T., Bergstra, J., Hunsberger, E., DeWolf, T., Stewart, T. C., Rasmussen, D., Choo, X., Voelker, A., and Eliasmith, C. Nengo: a Python tool for building large-scale functional brain models. *Frontiers in neuroinformatics*, 7:48, 2014.
- Bellec, G., Salaj, D., Subramoney, A., Legenstein, R., and Maass, W. Long short-term memory and learning-to-learn in networks of spiking neurons. In *Advances in Neural Information Processing Systems*, pp. 787–797, 2018.
- Blouw, P., Choo, X., Hunsberger, E., and Eliasmith, C. Benchmarking keyword spotting efficiency on neuromorphic hardware. In *Proceedings of the 7th Annual Neuro-inspired Computational Elements Workshop*, pp. 1–8, 2019.
- Chandar, S., Sankar, C., Vorontsov, E., Kahou, S. E., and Bengio, Y. Towards non-saturating recurrent units for modelling long-term dependencies. *arXiv preprint arXiv:1902.06704*, 2019.
- Chklovskii, D. B. and Soudry, D. Neuronal spike generation mechanism as an oversampling, noise-shaping A-to-D converter. In *Advances in Neural Information Processing Systems*, pp. 503–511, 2012.
- Courbariaux, M., Bengio, Y., and David, J.-P. BinaryConnect: Training deep neural networks with binary weights during propagations. In *Advances in Neural Information Processing Systems*, pp. 3123–3131, 2015.
- Davies, M., Srinivasa, N., Lin, T.-H., Chinya, G., Cao, Y., Choday, S. H., Dimou, G., Joshi, P., Imam, N., Jain, S., et al. Loihi: A neuromorphic manycore processor with on-chip learning. *IEEE Micro*, 38(1):82–99, 2018.
- Dayan, P. and Abbott, L. F. *Theoretical neuroscience: computational and mathematical modeling of neural systems*. MIT press, 2001.
- Floyd, R. and Steinberg, L. An adaptive technique for spatial grayscale. In *Proceedings of the Society of Information Display*, volume 17, pp. 75–77, 1976.
- Furber, S. B., Galluppi, F., Temple, S., and Plana, L. A. The SpiNNaker project. *Proceedings of the IEEE*, 102(5): 652–665, 2014.
- Ginsburg, B., Nikolaev, S., Kiswani, A., Wu, H., Gholaminejad, A., Kierat, S., Houston, M., and Fit-Florea, A. Tensor processing using low precision format, December 28 2017. US Patent App. 15/624,577.
- Glorot, X. and Bengio, Y. Understanding the difficulty of training deep feedforward neural networks. In *Proceedings of the Thirteenth International Conference on Artificial Intelligence and Statistics*, pp. 249–256, 2010.
- Gupta, S., Agrawal, A., Gopalakrishnan, K., and Narayanan, P. Deep learning with limited numerical precision. In *International Conference on Machine Learning*, pp. 1737–1746, 2015.
- Hopkins, M., Mikaitis, M., Lester, D. R., and Furber, S. Stochastic rounding and reduced-precision fixed-point arithmetic for solving neural ODEs. *arXiv preprint arXiv:1904.11263*, 2019.
- Hua, W., Zhou, Y., De Sa, C. M., Zhang, Z., and Suh, G. E. Channel gating neural networks. In *Advances in Neural Information Processing Systems*, pp. 1884–1894, 2019.
- Huh, D. and Sejnowski, T. J. Gradient descent for spiking neural networks. In *Advances in Neural Information Processing Systems*, pp. 1433–1443, 2018.
- Hunsberger, E. and Eliasmith, C. Spiking deep networks with LIF neurons. *arXiv preprint arXiv:1510.08829*, 2015.
- Jacob, B., Kligys, S., Chen, B., Zhu, M., Tang, M., Howard, A., Adam, H., and Kalenichenko, D. Quantization and training of neural networks for efficient integer-arithmetic-only inference. In *Proceedings of the IEEE Conference on Computer Vision and Pattern Recognition*, pp. 2704–2713, 2018.
- Jouppi, N. P., Young, C., Patil, N., Patterson, D., Agrawal, G., Bajwa, R., Bates, S., Bhatia, S., Boden, N., Borchers, A., et al. In-datacenter performance analysis of a Tensor Processing Unit. In *Proceedings of the 44th Annual International Symposium on Computer Architecture*, pp. 1–12, 2017.
- Kingma, D. P. and Ba, J. Adam: A method for stochastic optimization. *arXiv preprint arXiv:1412.6980*, 2014.
- Koch, C. *Biophysics of computation: information processing in single neurons*. Oxford university press, 2004.
- Krithivasan, S., Sen, S., Venkataramani, S., and Raghunathan, A. Dynamic spike bundling for energy-efficient

- spiking neural networks. In *International Symposium on Low Power Electronics and Design*, pp. 1–6. IEEE, 2019.
- Le, Q. V., Jaitly, N., and Hinton, G. E. A simple way to initialize recurrent networks of rectified linear units. *arXiv preprint arXiv:1504.00941*, 2015.
- Legendre, A.-M. Recherches sur l’attraction des sphéroïdes homogènes. *Mémoires de Mathématiques et de Physique, présentés à l’Académie Royale des Sciences*, pp. 411–435, 1782.
- Li, M., Li, Y., Chuang, P., Lai, L., and Chandra, V. Improving efficiency in neural network accelerator using operands hamming distance optimization. In *The 5th Workshop on Energy Efficient Machine Learning and Cognitive Computing. EMC2*, 2019.
- Liu, C., Bellec, G., Vogginger, B., Kappel, D., Partzsch, J., Neumärker, F., Höppner, S., Maass, W., Furber, S. B., Legenstein, R., and Mayr, C. G. Memory-efficient deep learning on a SpiNNaker 2 prototype. *Frontiers in neuroscience*, 12:840, 2018.
- McKinstry, J. L., Esser, S. K., Appuswamy, R., Bablani, D., Arthur, J. V., Yildiz, I. B., and Modha, D. S. Discovering low-precision networks close to full-precision networks for efficient embedded inference. *arXiv preprint arXiv:1809.04191*, 2018.
- Moloney, D. Embedded deep neural networks: “The cost of everything and the value of nothing”. In *Hot Chips 28 Symposium*, pp. 1–20. IEEE, 2016.
- Moreira, O., Yousefzadeh, A., Chersi, F., Kapoor, A., Zwartenkot, R.-J., Qiao, P., Cinserin, G., Khoei, M. A., Lindwer, M., and Tapson, J. NeuronFlow: A hybrid neuromorphic – dataflow processor architecture for AI workloads. In *2nd IEEE International Conference on Artificial Intelligence Circuits and Systems*. IEEE, 2020.
- Nayak, P., Zhang, D., and Chai, S. Bit efficient quantization for deep neural networks. *arXiv preprint arXiv:1910.04877*, 2019.
- Neckar, A., Fok, S., Benjamin, B. V., Stewart, T. C., Oza, N. N., Voelker, A. R., Eliasmith, C., Manohar, R., and Boahen, K. Braindrop: A mixed-signal neuromorphic architecture with a dynamical systems-based programming model. *Proceedings of the IEEE*, 107(1):144–164, 2018.
- Pei, J., Deng, L., Song, S., Zhao, M., Zhang, Y., Wu, S., Wang, G., Zou, Z., Wu, Z., He, W., et al. Towards artificial general intelligence with hybrid Tianjic chip architecture. *Nature*, 572(7767):106–111, 2019.
- Rasmussen, D. NengoDL: Combining deep learning and neuromorphic modelling methods. *Neuroinformatics*, 17(4):611–628, 2019.
- Rodrigues, O. *De l’attraction des sphéroïdes, Correspondence sur l’É-cole Impériale Polytechnique*. PhD thesis, Thesis for the Faculty of Science of the University of Paris, 1816.
- Situnayake, D. and Warden, P. *TinyML: Machine Learning with TensorFlow Lite on Arduino and Ultra-Low Power Microcontrollers*. O’Reilly Media, Inc., 2019. ISBN 9781492052036.
- Srivastava, N., Hinton, G., Krizhevsky, A., Sutskever, I., and Salakhutdinov, R. Dropout: A simple way to prevent neural networks from overfitting. *The journal of machine learning research*, 15(1):1929–1958, 2014.
- Stöckl, C. and Maass, W. Recognizing images with at most one spike per neuron. *arXiv preprint arXiv:2001.01682*, 2019.
- Sze, V., Chen, Y.-H., Yang, T.-J., and Emer, J. S. Efficient processing of deep neural networks: A tutorial and survey. *Proceedings of the IEEE*, 105(12):2295–2329, 2017.
- Voelker, A., Kajić, I., and Eliasmith, C. Legendre Memory Units: Continuous-time representation in recurrent neural networks. In *Advances in Neural Information Processing Systems*, pp. 15544–15553, 2019.
- Voelker, A. R. *Dynamical Systems in Spiking Neuromorphic Hardware*. Phd thesis, University of Waterloo, 2019.
- Voelker, A. R. Methods and systems for training multi-bit spiking neural networks for efficient implementation on digital hardware. *US Patent App. 17/086,218 (patent pending)*, 10 2020.
- Voelker, A. R. and Eliasmith, C. Improving spiking dynamical networks: Accurate delays, higher-order synapses, and time cells. *Neural computation*, 30(3):569–609, 2018.
- Wang, D., Li, M., Wu, L., Chandra, V., and Liu, Q. Energy-aware neural architecture optimization with fast splitting steepest descent. *arXiv preprint arXiv:1910.03103*, 2019.
- Yadav, C. and Bottou, L. Cold case: The lost MNIST digits. In *Advances in Neural Information Processing Systems*, pp. 13443–13452, 2019.
- Yoon, Y. C. LIF and simplified SRM neurons encode signals into spikes via a form of asynchronous pulse sigma–delta modulation. *IEEE transactions on neural networks and learning systems*, 28(5):1192–1205, 2016.
- Yousefzadeh, A., Hosseini, S., Holanda, P., Leroux, S., Werner, T., Serrano-Gotarredona, T., Barranco, B. L., Dhoedt, B., and Simoens, P. Conversion of synchronous artificial neural network to asynchronous spiking neural

network using sigma-delta quantization. In *1st IEEE International Conference on Artificial Intelligence Circuits and Systems*, pp. 81–85. IEEE, 2019a.

Yousefzadeh, A., Khoei, M. A., Hosseini, S., Holanda, P., Leroux, S., Moreira, O., Tapson, J., Dhoedt, B., Simoens, P., Serrano-Gotarredona, T., et al. Asynchronous spiking neurons, the natural key to exploit temporal sparsity. *IEEE Journal on Emerging and Selected Topics in Circuits and Systems*, 9(4):668–678, 2019b.

Zhang, W. and Li, P. Spike-train level backpropagation for training deep recurrent spiking neural networks. In *Advances in Neural Information Processing Systems*, pp. 7800–7811, 2019.

Zhang, Y., Suda, N., Lai, L., and Chandra, V. Hello edge: Keyword spotting on microcontrollers. *arXiv preprint arXiv:1711.07128*, 2017.

Zhu, M. and Gupta, S. To prune, or not to prune: exploring the efficacy of pruning for model compression. *arXiv preprint arXiv:1710.01878*, 2017.

A Spike in Performance – Supplementary

Aaron R. Voelker, Daniel Rasmussen, and Chris Eliasmith

February 10, 2020

1. Introduction

For clarity, we restate Algorithm 1 from the main article with some additional annotations. This algorithm quantizes an activation function, f , given a parameter $\omega > 0$ that acts as a time-step. For convenience, we assume the range of f is scaled such that $|f(\cdot)| \leq 1$ over the domain of valid inputs. This may be accomplished by fusing a normalization term with the weights, or by clipping or saturating the nonlinearity. The ideal output of the activation function at step t is defined as $a_t = f(x_t)$. The algorithm maintains one scalar state-variable per neuron, $v_{t-1} \mapsto v_t$ (i.e., from one step to the next), initialized by sampling $v_0 \sim \mathcal{U}[0, 1)$.

Algorithm 1
Temporally-Diffused Quantizer ($f; \omega$)

Input: x_t

State: v_t

Output: \tilde{a}_t

$$\begin{aligned} s_t &\leftarrow v_{t-1} + \overbrace{f(x_t) \times \omega}^{c_t} \\ k_t &\leftarrow \lfloor s_t \rfloor \\ v_t &\leftarrow s_t - k_t \\ \tilde{a}_t &\leftarrow k_t / \omega \end{aligned}$$

Let $c_t = f(x_t) \times \omega$, since this term will appear frequently, and (as we will see) corresponds to the expected spike count. We'll also regularly use the facts that $k_t = \lfloor s_t \rfloor = \lfloor v_{t-1} + f(x_t) \times \omega \rfloor = \lfloor v_{t-1} + c_t \rfloor$, $f(x_t) = a_t = c_t / \omega$, and $0 \leq v_t < 1$ for all $t \in \mathbb{N}$.

Section 2 restates and then proves each property from the main article (and in a slightly different order). Section 3 provides some empirical justification for the useful assumption that the neurons' voltages, v_t , remain uniformly distributed in practice. Section 4 details how we scale and bias the leaky integrate-and-fire (LIF) response curve.

2. Statements and Proofs

Theorem 1 (Zero-Mean Error). *Supposing $v_{t-1} \sim \mathcal{U}[0, 1]$, the expected quantization error is $\mathbb{E}[\tilde{a}_t - a_t] = 0$.*

Proof. Let $b_t = 1 - (c_t - \lfloor c_t \rfloor) = \lfloor 1 + c_t \rfloor - c_t$ correspond to the point at which $v_{t-1} + c_t$ floors down to $\lfloor c_t \rfloor$ for $v_{t-1} < b_t$, and otherwise $\lfloor 1 + c_t \rfloor$ for $v_{t-1} \geq b_t$. By the law of the unconscious statistician:

$$\begin{aligned} \mathbb{E}[\tilde{a}_t - a_t] &= \int_0^1 (\tilde{a}_t - a_t) dv_{t-1} \\ &= \omega^{-1} \int_0^1 (\lfloor v_{t-1} + c_t \rfloor - c_t) dv_{t-1} \\ &= \omega^{-1} \left[\int_0^{b_t} (\lfloor v_{t-1} + c_t \rfloor - c_t) dv_{t-1} + \int_{b_t}^1 (\lfloor v_{t-1} + c_t \rfloor - c_t) dv_{t-1} \right] \\ &= \omega^{-1} \left[\int_0^{b_t} (\lfloor c_t \rfloor - c_t) dv_{t-1} + \int_{b_t}^1 (\lfloor 1 + c_t \rfloor - c_t) dv_{t-1} \right] \\ &= \omega^{-1} [b_t(b_t - 1) + (1 - b_t)b_t] \\ &= 0. \end{aligned}$$

□

Corollary 1 (Expected Spike Count). $\mathbb{E}[k_t] = c_t$, hence c_t corresponds to the expected number of spikes (positive or negative) across a time window of length ω .

Proof. By linearity of expectation, and since $\mathbb{E}[\tilde{a}_t] = a_t = f(x_t)$,

$$\mathbb{E}[k_t] = \mathbb{E}[k_t/\omega] \times \omega = a_t \times \omega = c_t.$$

□

Corollary 2 (Temporal Sparsity). *The spike count scales as $\mathcal{O}(\omega)$.*

Proof. Since $|f(\cdot)| \leq 1$ is $\mathcal{O}(1)$, we have k_t scaling as $\mathcal{O}(c_t) = \mathcal{O}(\omega)$.

□

Theorem 2 (Bounded Error). *The total quantization error is bounded by $|\sum_{t \in T} \tilde{a}_t - a_t| < \omega^{-1}$ across any consecutive slice of time-steps, T .*

Proof. Suppose T is the discrete interval $[i+1, j]$, for natural numbers $i < j$. Using the fact that $\tilde{a}_t = k_t/\omega = (s_t - v_t)/\omega = (v_{t-1} + c_t - v_t)/\omega$, we obtain a telescoping sum:

$$\begin{aligned} \sum_{t \in T} \tilde{a}_t - a_t &= \omega^{-1} \left(\sum_{t=i+1}^j (v_{t-1} + c_t - v_t) - c_t \right) \\ &= \omega^{-1} \left(\sum_{t=i+1}^j v_{t-1} - v_t \right) \\ &= \omega^{-1}(v_i - v_j). \end{aligned}$$

Since $0 \leq (v_i, v_j) < 1$, this implies $|v_i - v_j| < 1$ and therefore $|\sum_{t \in T} \tilde{a}_t - a_t| < \omega^{-1}$.

□

Corollary 3 (ANN Regime). *As $\omega \rightarrow \infty$, $\tilde{a}_t \rightarrow a_t$, hence the activation function becomes equivalent to the ideal $f(\cdot)$.*

Proof. As a corollary to Theorem 2 with $T = \{t\}$, $\tilde{a}_t \rightarrow a_t$ in the limit of $\omega \rightarrow \infty$.

□

Corollary 4 (Backpropagation Training). *Assuming $(v_{t-1}, v_t) \sim \mathcal{U}[0, 1)$ are independent random variables, we have $\tilde{a}_t = a_t + \eta$ where $\eta \sim \mathcal{T}(-\omega^{-1}, \omega^{-1})$ is zero-mean noise with a symmetric triangular distribution. This justifies assigning a gradient of zero to η during the backwards pass of the backpropagation algorithm.*

Proof. Consider any t , and apply Theorem 2 with $T = \{t\}$ to get $\eta = \tilde{a}_t - a_t = \omega^{-1} (v_{t-1} - v_t)$, which is the scaled difference between two independently distributed uniform random variables. This results in the standard triangular distribution, symmetric about zero, and divided by ω . We briefly note that the covariance in η from one time-step to the next is:

$$\text{cov}(\omega^{-1} (v_{t-1} - v_t), \omega^{-1} (v_t - v_{t+1})) = \omega^{-2} \left(\frac{1}{4} - \frac{1}{4} - \frac{1}{3} + \frac{1}{4} \right) = -1/(12\omega^2).$$

□

Corollary 5 (Signal-to-Noise Ratio). *Supposing $\mathbb{E}[\tilde{a}_t - a_t] = 0$, the signal-to-noise ratio (SNR) of \tilde{a}_t scales as $\Omega(\omega)$.*

Proof. Since the signal has zero-mean error (by assumption), the SNR, defined as the ratio of the signal to the standard deviation of its error, is:

$$\text{SNR} = \frac{a_t}{\sqrt{\mathbb{E}[(\tilde{a}_t - a_t)^2]}}.$$

Popoviciu's inequality, applied to Theorem 2 with $T = \{t\}$, gives the bound:

$$\sqrt{\mathbb{E}[(\tilde{a}_t - a_t)^2]} \leq \frac{1}{2} (\omega^{-1} - (-\omega^{-1})) = \omega^{-1}.$$

Hence, $\text{SNR} \geq a_t \omega = \Omega(\omega)$. Furthermore, we remark that assuming $v_{t-1} \sim \mathcal{U}[0, 1)$ leads to a stronger bound (by a factor of 2). In particular, using this assumption, the variance term can be derived similarly to the zero-mean error, while using the fact that $0 < b_t \leq 1$ to establish a tighter upper-bound:

$$\begin{aligned} \mathbb{E}[(\tilde{a}_t - a_t)^2] &= \int_0^1 (\tilde{a}_t - a_t)^2 dv_{t-1} \\ &= \omega^{-2} \left[\int_0^{b_t} ([c_t] - c_t)^2 dv_{t-1} + \int_{b_t}^1 ([1 + c_t] - c_t)^2 dv_{t-1} \right] \\ &= \omega^{-2} [b_t(b_t - 1)^2 + (1 - b_t)b_t^2] \\ &= \omega^{-2} (b_t(1 - b_t)) \\ &\leq \left(\frac{1}{2\omega} \right)^2. \end{aligned}$$

Hence, $\text{SNR} \geq 2a_t \omega = \Omega(\omega)$. □

Theorem 3 (Synaptic Filtering). *The SNR from Corollary 5 may be further scaled by the time-constant of a lowpass filter. Specifically, supposing $\mathbb{E}[\tilde{a}_t - a_t] = 0$, the SNR is $\geq \omega/(1 - e^{-1/\bar{\tau}}) = \Omega(\omega\bar{\tau})$ where $\bar{\tau} = \tau/dt$ is the discrete time-constant of the zero-order hold (ZOH) lowpass filter applied to \tilde{a} .*

Proof. Intuitively, when \tilde{a} is filtered by a first-order lowpass filter, the quantization errors cancel out in a similar manner to Theorem 2, which boosts the SNR by the time-constant of the filter. While it is possible to give a much more general result, we instead prove this in a direct and self-contained manner. We note that by linearity of convolution, it does not functionally matter whether we apply the filter before or after the connection weight-matrix.

First, we simply state that ZOH-discretizing a first-order lowpass filter with a continuous-time impulse response of $h(t) = \tau^{-1}e^{-t/\tau}$ ($t \geq 0$), with a time-step of dt , results in the discrete-time impulse response of:

$$h_t = \left(1 - e^{-1/\bar{\tau}}\right) e^{-t/\bar{\tau}}, \quad t \in \mathbb{N}.$$

For completeness, we note that, in the Laplace domain, $H(s) = 1/(\tau s + 1)$ and:

$$H(z) = \frac{1 - e^{-1/\bar{\tau}}}{z - e^{-1/\bar{\tau}}}.$$

Second, the quantity of interest—the filtered error at step t —is the following discrete-time convolution:

$$((\tilde{a} - a) * h)_t \stackrel{\text{DEF}}{=} \sum_{i=0}^{\infty} (\tilde{a}_{t-i} - a_{t-i}) h_i,$$

where negative indices are handled appropriately by setting those values to zero. Third, we note that $h_{i-1} > h_i$ for all $i > 0$. Fourth, $1 - e^{-y} < y$ for any $y > 0$ ($y = 1/\bar{\tau}$ in particular). We are now ready to bound the filtered error:

$$\begin{aligned} |((\tilde{a} - a) * h)_t| &= \left| \sum_{i=0}^{\infty} (\tilde{a}_{t-i} - a_{t-i}) h_i \right| \\ &= \omega^{-1} \left| \sum_{i=0}^{\infty} (v_{t-i-1} - v_{t-i}) h_i \right| \\ &= \omega^{-1} \left| -h_0 v_t + \sum_{i=1}^{\infty} (h_{i-1} - h_i) v_{t-i} \right| \\ &< \omega^{-1} \max \left(h_0, \sum_{i=1}^{\infty} h_{i-1} - h_i \right) \\ &= \omega^{-1} \max \left((1 - e^{-1/\bar{\tau}}), (1 - e^{-1/\bar{\tau}}) \sum_{i=1}^{\infty} e^{-(i-1)/\bar{\tau}} - e^{-i/\bar{\tau}} \right) \\ &= \omega^{-1} (1 - e^{-1/\bar{\tau}}) \max \left(1, (e^{1/\bar{\tau}} - 1) \sum_{i=1}^{\infty} e^{-i/\bar{\tau}} \right) \\ &= \omega^{-1} (1 - e^{-1/\bar{\tau}}) \max \left(1, (e^{1/\bar{\tau}} - 1) \frac{1}{e^{1/\bar{\tau}} - 1} \right) \\ &= \omega^{-1} (1 - e^{-1/\bar{\tau}}) \\ &< \frac{1}{\omega \bar{\tau}}. \end{aligned}$$

We remark that the third line is equivalent in the \mathcal{Z} -domain to multiplying $(z^{-1} - 1)H(z)$ with the \mathcal{Z} -transform of v . Although it is once again possible to obtain tighter bounds by assuming uniform voltages, simply applying Popoviciu's inequality produces the filtered SNR $\geq (a * h)_t \omega / (1 - e^{-1/\bar{\tau}}) = \Omega(\omega \bar{\tau})$. \square

Lemma 1 (Bit-Width). *The number of bits required to represent \tilde{a}_t in binary is at most $\lceil \log_2(\omega + 1) \rceil$ if f is non-negative (plus a sign bit if f can be negative).*

Proof. If f is non-negative, then k_t can take on $\omega + 1$ different values (specifically, $k_t \in [0, \omega]$). Representing $\omega + 1$ distinct values in binary requires $\lceil \log_2(\omega + 1) \rceil$ bits in the worst case. If f can be negative, then k_t can take on discrete values across the interval $[-\omega, \omega]$ and thus an additional sign bit is required. \square

Corollary 6 (SNN Regime). *When $\omega \leq 1$, the activation function becomes a conventional spiking neuron since it outputs either zero or a spike (ω^{-1}) if f is non-negative (and optionally a negative spike if f is allowed to be negative).*

Proof. As a corollary to Lemma 1, a choice of $\omega \leq 1$ results in activities that can be represented using at most one bit if f is non-negative (and optionally a sign bit if f is allowed to be negative). Hence the neuron model can only signal events (i.e., “spikes”) for non-negative response functions, and optionally negative spikes for signed response functions. \square

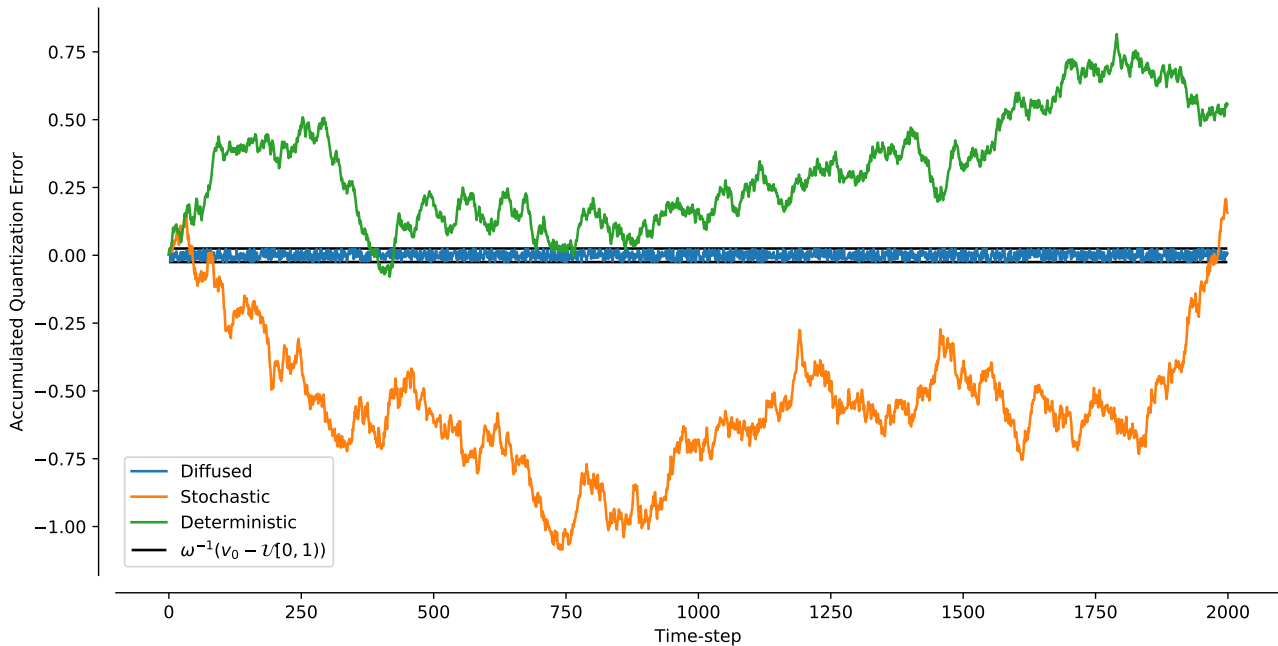


Figure 4: Numerical validation of Theorem 2 given a random input signal, and compared to the accumulated error for two alternative quantizers: a deterministic quantizer that does not temporally-diffuse its error, and a non-deterministic quantizer that uses stochastic rounding. The voltage is initialized to $v_0 = 0.5$ in this case. It is especially important to keep the total quantization error bounded when considering Recurrent Neural Networks (RNNs), since they tend to accumulate and propagate their errors over time.

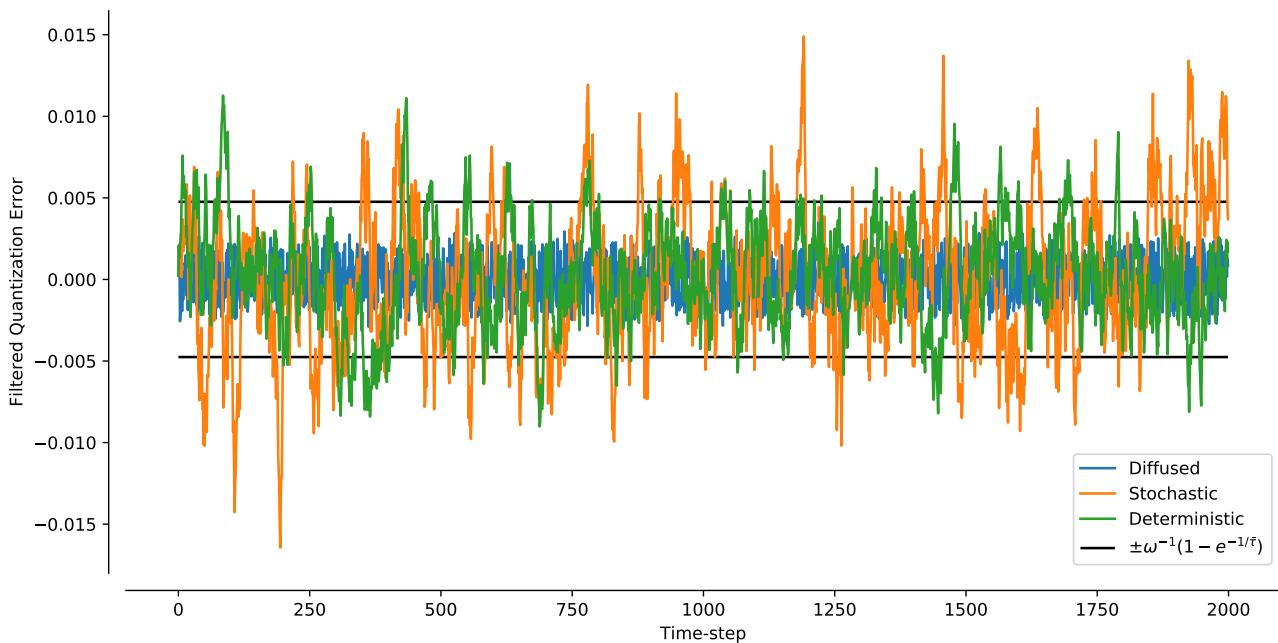


Figure 5: Numerical validation of Theorem 3 ($\bar{\tau} = 10$) given the same input signal from Figure 4, and compared to the filtered error for the same two alternative quantizers.

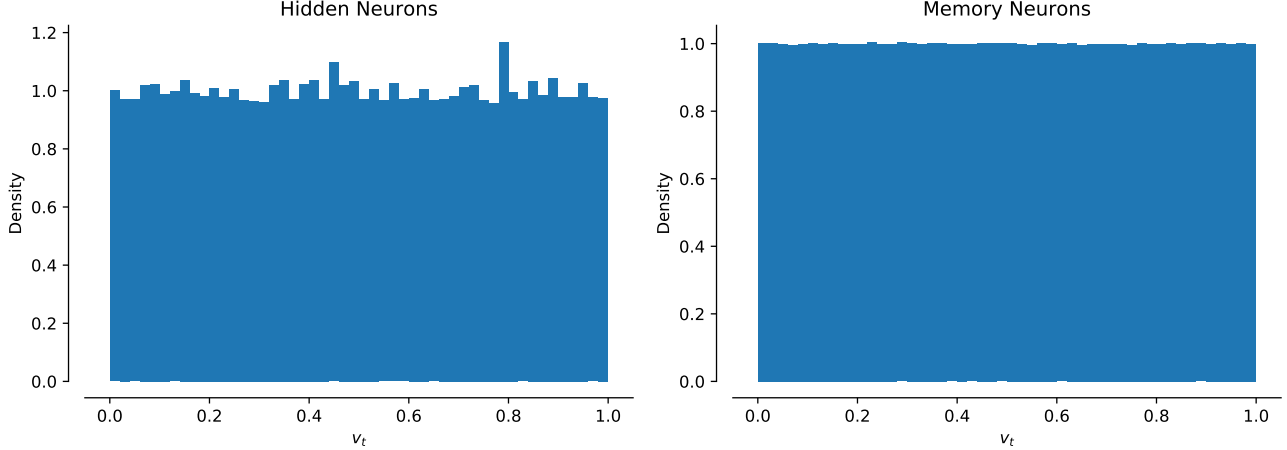


Figure 6: Distribution of neuron state-variables (v_t) for the Hybrid-Spiking Legendre Memory Unit (hsLMU) network solving the psMNIST task (see main article). Histograms (bin-width of 0.02) are provided for the hidden neurons ($f_h(\cdot)$; Left) and the memory neurons ($f_m(\cdot)$; Right). Data is collected for all $t \in [1, 784]$ steps across the first 500 test digits.

3. Uniform Voltages

Empirically, and in practice, we found that the neurons’ voltages (v_t) tend to remain uniformly distributed over time. Specifically, for benchmarks that we explored, v_t is well-approximated as $\mathcal{U}[0, 1)$ – especially so for the memory neurons (see Figure 6 for example).

To quantify the assumption of uniformity, we performed two-sided Kolmogorov-Smirnov tests for goodness of fit. The hidden neurons had an empirical CDF that was no more than 0.3% different from that of the exact uniform distribution, while the memory neurons had an empirical CDF that was no more than 0.03% different (KS-statistics < 0.003 and 0.0003 , respectively, with p -values $< 10^{-7}$). Thus, the uniform assumption (used only by Theorem 1 and its dependent claims) holds approximately for both populations.

To quantify the stronger assumption that the voltages are also independently distributed from one time-step to the next, we measured the sample covariance between v_{t-1} and v_t . Although uncorrelatedness does not imply independence, we found that the memory layer had a covariance that is $\approx 1,380\times$ smaller than its variance. In contrast, the hidden layer only had a covariance that is $\approx 1.25\times$ smaller than its variance. Thus, the independence assumption (used only by Corollary 4) does not hold very well for the hidden layer, as its quantization errors are correlated in time. We suspect that the temporal covariance in the hidden neurons is due to these neurons being driven by low-frequency inputs close to zero, versus the inputs to the memory neurons being sufficiently decorrelated in time.

4. LIF Normalization

For the hidden layer, $f_h(\cdot)$, we use the leaky integrate-and-fire (LIF) neuron model with a leak of $\bar{\tau}_{rc} = 10$ time-steps and a refractory period of $\bar{\tau}_{ref} = 1$ time-step—corresponding to Nengo’s defaults given a time-step of 2 ms—such that its time-averaged response curve is:¹

$$f_h(x_t) = \frac{1}{\bar{\tau}_{ref} + \bar{\tau}_{rc} \log_{1p} \left(\frac{1}{\alpha x_t + \beta} \right)}, \quad 0 \leq f_h(x_t) < 1,$$

where (α, β) are constants that scale and shift the curve. Specifically, we bias the input such that $f_h(x_t) = 0 \iff x_t \leq 0$, and scale it such that $f_h(1) = r \stackrel{\text{DEF}}{=} e/(1+e)$. This is achieved by choosing:

$$\alpha = - \left[\exp_{1p} \left(\frac{\bar{\tau}_{ref} - 1/r}{\bar{\tau}_{rc}} \right) \right]^{-1} - 1 = - \left[\exp_{1p} \left(\frac{\bar{\tau}_{ref} - (1+e)/e}{\bar{\tau}_{rc}} \right) \right]^{-1} - 1,$$

¹ $\log_{1p}(x) = \ln(1+x)$ and $\exp_{1p}(x) = \exp(x) - 1$ are standard nonlinearities in NumPy and TensorFlow.

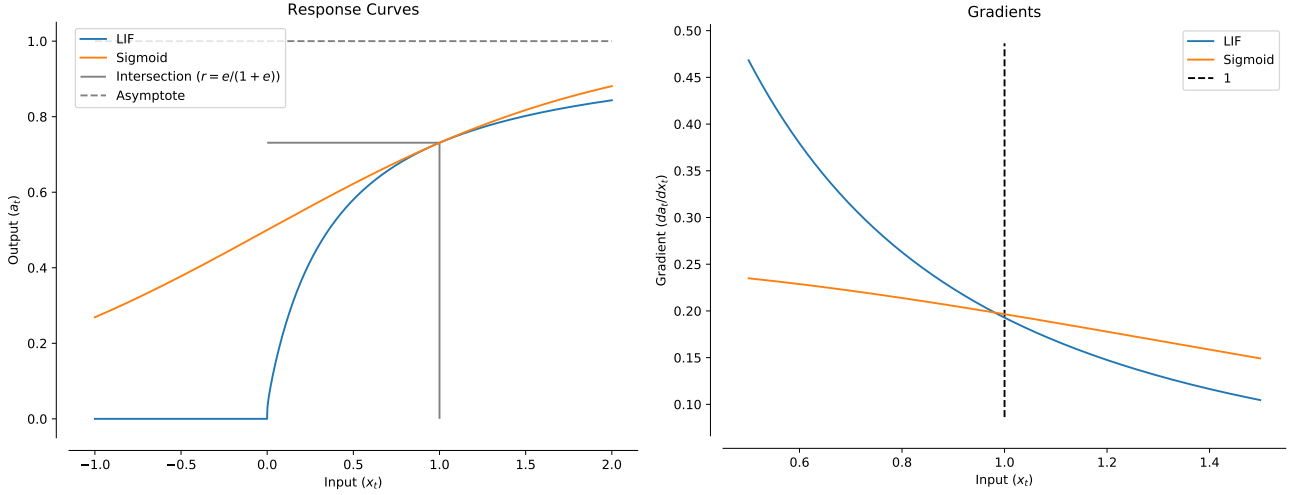


Figure 7: The leaky integrate-and-fire (LIF) with discrete time-constants $(\bar{\tau}_{rc}, \bar{\tau}_{ref}) = (10, 1)$ and a gain and bias of (α, β) such that $0 \leq f_h(x_t) < 1$, $f_h(x_t) = 0 \iff x_t \leq 0$, and $\omega = 1$ corresponds to a biological time-step of 2 ms. (Left) The response curve is scaled such that $f_h(1) = \text{sigmoid}(1) = r = e/(1 + e)$. (Right) The gradients are also approximately equal at $x_t = 1$, and become identical in the limit of $\bar{\tau}_{rc} \rightarrow \infty$.

and $\beta = 1$. Since (α, β) are constants, they can be fused with existing parameters in the final network, in particular by multiplying the incoming weights with α and adding β to the incoming bias parameters.

The above “time-normalized LIF” is convenient for two reasons. The first reason is that the nonlinearity becomes normalized to $0 \leq f_h(x_t) < 1$, such that a value of $\omega = 1$ corresponds to a spiking LIF model with a biological time-step of 2 ms, analogous to a conventional LIF neuron model that spikes at most once per step. The second reason is that $f_h(1) = \text{sigmoid}(1) = r$, and so the model has a similar dynamic range to the $\text{sigmoid}(\cdot)$ activation (see Figure 7), making it somewhat more compatible with weight initialization methods designed for sigmoidal layers. We also note that the gradients of f_h and sigmoid are approximately the same at 1, and become equal as $\bar{\tau}_{rc}$ increases.